Chemical Physics 399 (2012) 86–93

Contents lists available at SciVerse ScienceDirect

Chemical Physics

journal homepage: www.elsevier.com/locate/chemphys

A theoretical study on electronic predissociation in the $NeBr_2$ van der Waals molecule

Ramón Hernández-Lamoneda [a], Cristina Sanz-Sanz [b], Octavio Roncero [b], Jordan M. Pio [c], Molly A. Taylor [c], Kenneth C. Janda [c,*]

[a] Centro de Investigaciones Químicas, Universidad Autónoma de Morelos, A venida Universidad 1001, Cuernavaca, Morelos 62210, Mexico
[b] Instituto de Física Fundamental, CSIC, Serrano 123, 28006 Madrid, Spain
[c] Department of Chemistry and Institute of Surface and Interface Science, University of California, Irvine, CA 92697-2025, USA

ARTICLE INFO

Article history:
Available online 22 September 2011

Keywords:
van der Waals clusters
Electronic predissociation
Vibrational predissociation
Rare gas halogen clusters

ABSTRACT

We present the first comprehensive *ab initio* study of the Ne–Br_2 potential energy surfaces and the nonadiabatic couplings between the valence excited electronic states. These *ab initio* results are used to obtain 3-D approximate potentials for each electronic state, and these potentials are used in a wave packet calculation of the competing electronic predissociation and vibrational predissociation dynamics. The results of this calculation are in excellent agreement with both experimental results and a previous empirical fit to the experiments. The calculations allow us to observe not only the competition between vibrational and electronic dynamics for the dimer, but also the competition between two different electronic channels. Coupling to the 2_g state dominates for the levels studied here, but coupling to the *C* state is progressively more important for low vibrational levels, and may dominate at levels below which the current results pertain. The ability of *ab initio* surfaces and couplings to so accurately reproduce experimental data raises the hope of a complete understanding of the VP and EP dynamics for other Rg-halogen dimers. Success in the case presented here is largely due to the fact that the VP dynamics for the vibrational levels in this study are in the simple, direct regime. Understanding the simple case so thoroughly provides new hope that the more complicated examples, such as ArI_2 and $NeCl_2$, for which experiment and theory are not currently in accord, may yet yield to analysis.

1. Introduction

The accurate description of excited state potential energy surfaces (PES) and dynamics is a major challenge for theoretical chemistry. The rare gas-halogen dimers (RgX_2) are excellent model systems for this type of study. Their small size makes these complexes amenable to very detailed study, and because they have only a small number of degrees of freedom, there are only a few dissociation pathways [1]. One of these is nonadiabatic electronic predissociation (EP) induced by the rare gas atom. As will be discussed later, EP dynamics have been observed in this type of complex as a result of coupling between the bound *B* electronic state of the X_2 molecule and one or more of the dissociative states that cross it to form: $Rg + X(^2P_{3/2}) + X(^2P_{3/2})$ [2–5]. In the case of the rare gas-halogens, the EP process competes only with vibrational predissociation (VP), a process where one or more quanta of vibrational energy is transferred from the $X_2(B, v')$ subunit to the van der Waals mode, dissociating the rare gas atom to form: $Ne + X_2(B, v'' < v')$. The VP dynamics can be quite simple, as in the case of direct VP, or more complicated as with intra-molecular vibrational relaxation (IVR) [6].

The dynamics of rare gas halogens have been studied in great detail spectroscopically [1,8,9]. In experiments, the $X_2(B, v')$ product of VP can be easily detected by laser induced fluorescence. The presence of a competing EP pathway has so far only been inferred from the depletion of this fluorescence. There are two major difficulties that have prevented good agreement between experiment and theory on the VP/EP competition in previous studies. One, the EP is often in competition with VP proceeding via IVR, which is much more difficult to model and also can lead to weak spectral features and oscillation in the predissociation lifetimes, making it difficult to untangle the relative contributions of EP and VP [5,10]. Second, since the experiments rely on the formation of the product of VP, there is no experimental signature of EP (other than the absence of signal) when EP is the dominant pathway.

The ArI_2 complex is the first system for which competing EP and VP dynamics have been observed over a wide range of *B* state vibrational levels. The competing EP pathway was inferred from oscillations in the I_2 fluorescence intensity as a function of *B* state vibrational level between $v' = 12$ and 26 [2]. Although VP

* Corresponding author.
E-mail address: kcjanda@uci.edu (K.C. Janda).

0301-0104/$ - see front matter © 2011 Elsevier B.V. All rights reserved.
doi:10.1016/j.chemphys.2011.09.015

probabilities $\left(\frac{k_{VP}}{k_{VP}+k_{EP}}\right)$ have been measured by the simultaneous measurement of absorption and fluorescence excitation spectra [11], measurements of the total predissociation rates ($k_{VP} + k_{EP}$) have only been done for two levels, $v' = 18$ and 21 [12]. Therefore, individual EP and VP rates could be extracted only for those two levels. However, the authors in Ref. [11] estimated separate VP and EP rates for $16 \leqslant v' \leqslant 24$ by assuming that the VP lifetime decreases linearly with vibrational quantum number.

One issue that complicates the dynamics for the ArI_2 complex is that in the $v' = 16$–23 interval, VP occurs by the transfer of three vibrational quanta sequentially via intermediate doorway states. From calculations on this system it was concluded that IVR in ArI_2 occurs in the sparse-intermediate regime and as a result the VP lifetimes oscillate as a function of vibrational level [13]. When compared to the oscillations in VP lifetimes, the oscillations in EP lifetimes, which were calculated using a time dependent golden rule treatment [4], were found to be much smaller. In recent calculations on the competition between VP and EP, it was once again found that the VP oscillations are larger [5,14]. Thus, details of the competition between VP and EP in ArI_2 remain an open problem, as was recently reviewed [10].

Most commonly either EP or VP dominates the dynamics, with one process being significantly faster than the other. When EP is the predominate pathway, no X_2 product is observed. For example, in the complexes of Xe and Kr with I_2, no I_2 product is observed [15], and for the complexes of Xe and Kr with Cl_2 VP products were only detected for a few vibrational levels [16,17]: $v' = 8$–11 for $KrCl_2$ [17], and $v' = 10$–11 for $XeCl_2$ [17]. In all these cases the most likely explanation for the dominance of the EP dynamics is that the coupling induced by these heavy rare gas atoms is large.

The $HeCl_2$ complex lies at the other extreme, with VP the predominate dissociation pathway for most vibrational levels. [18,19] In this case EP is expected to be quite weak since the He atom is so light and most likely induces only very weak coupling. For the complexes of the intermediately sized rare gases Ne and Ar with Cl_2, there is evidence of competition between EP and VP. For lower vibrational levels, VP dominates whereas for higher vibrational levels ($v' > 16$ for $NeCl_2$ [6,20,21], and $v' > 12$ for $ArCl_2$ [22]) no VP products are observed. Unlike the ArI_2 complex, there are no oscillations in the lifetimes. Instead, the signals disappear abruptly. The competition between EP and VP for these complexes was recently modeled theoretically [6] using *ab inito* estimates of the electronic couplings between the *B* and repulsive states [23]. The precise location where the repulsive 2_g state crosses the *B* state seems to determine at which v' the EP begins to dominate, but it was not possible to model quantitatively the appearance of the EP channel for the $NeCl_2$ complex.

Very recent experimental data on the predissociation of $NeBr_2$ [31] indicates that the predissociation dynamics of this complex may be much more amenable to the convergence of experimental results and theoretical calculations on the VP/EP competition. Due to the intermediate size of the Ne atom, the electronic coupling is significant, but not so large so as to completely quench the VP channel. Also, the repulsive state curve crossings occur low in the *B*-state potential, so that the EP is in competition with direct VP rather than IVR.

In this regard, the photodissociation dynamics of the $NeBr_2$ van der Waals cluster provides an interesting test case for theory. Only recently were these VP/EP competing dissociation pathways observed and characterized experimentally [31]. In the experimental study that prompted these calculations, the total predissociation rates ($k_{VP} + k_{EP}$) of the $NeBr_2$ complex were measured in real time as a function of v' in the range $v' = 10 - 20$ in the *B* electronic state. It was initially expected that $NeBr_2$ dissociated almost entirely via direct VP, in which case the rates would increase monotonically with increasing v' according to the energy gap law. Instead, the measured rates for the $NeBr_2$ complex show strong oscillations as a function of v'. These oscillations were attributed to a competing EP pathway, with the van der Waals interaction inducing a coupling between the Br_2 *B* state and one or more of the dissociative states that cross it.

It was proposed that the dependence of the EP rate on v' is mainly determined by the Franck–Condon factors between the Br_2 *B* state vibrational wavefunction and the isoenergetic product wavefunction for the repulsive electronic state responsible for EP. It was found that the v'-dependence of the Franck–Condon factors between the *B* and the $1_g/2_g$ states matched extremely well to that of the predissociation rate, and so the 1_g or 2_g states were likely responsible for the EP.

Recently, we performed full-dimensional wavepacket (WP) calculations of the $NeBr_2$ predissociation to test this Franck–Condon model [24]. In these calculations, we assumed a reasonable functional form for the dependence of the diabatic couplings between the *B* and $1_g/2_g$ states on the $NeBr_2$ geometry and scaled the couplings to achieve agreement between experimental and calculated predissociation rates. By including a small amount of coupling to the *C* state as well, the WP calculations achieved quantitative agreement with experiment.

This convergence of the experimental and calculated rates shows the initial proposal that the electronic coupling is mainly due to the $1_g/2_g$ states is very reasonable. However, other than the potential energy curve of the $1_g/2_g$ states, no *ab initio* data were used in these wave packet calculations. In particular, the couplings between the *B*, $1_g/2_g$, and *C* states were treated empirically, and the Ne–Br_2 interaction potential was assumed to be identical for all the electronic states.

In the present work, we use *ab initio* calculations to investigate many of the assumptions we made previously. We calculate the diabatic couplings between the *B* state and the repulsive states which cross it. We also calculate the van der Waals interaction potential for all the excited electronic states that participate in the EP of $NeBr_2$. Finally, using these *ab initio* data, we perform WP calculations again to see if the *ab initio* methods can reasonably describe the couplings and intermolecular interactions.

The accurate calculation of global excited state potential energy surfaces for weakly bound systems remains a challenging task for *ab initio* methodology. The standard methodology which has been applied successfully in the case of ground states is generally not applicable. In the case of the $NeBr_2$ system we want to treat highly stretched geometries for the diatom and include spin–orbit coupling effects in describing the low-lying excited states involved in the spectroscopy and dynamics of the complex. In the following section, we describe the methodologies used to calculate the non-adiabatic couplings and excited state intermolecular potentials and perform the WP calculations.

2. Calculation of the non-adiabatic couplings

We calculate non-adiabatic couplings between the *B* state and the repulsive states that participate in the $NeBr_2$ electronic predissociation (EP) using a procedure similar to that in our previous studies on EP in the Ne-and Ar–Cl_2 complexes [6]. The geometry of the complex is described by the Br-Br intramoleculer distance *r*, the distance between the Ne and Br_2 center-of-mass *R*, and the angle γ between the intra- and intermolecular bonds. For fixed values of *R* and γ, the potential energy curves of the relevant electronic states in *r* are calculated using the *ab initio* methods described below. The curves are calculated for $2.86 \leqslant r \leqslant 3.49$ Å, spanning the region where the repulsive states cross the attractive branch of the *B* state potential. As a result of the intermolecular

potential some of the diatomic crossings turn into avoided crossings of the associated potential energy surfaces. According to the *ab initio* calculations, the *C* and 2_g states are the only two states that have significant coupling with the *B* state and undergo avoided crossings in the range of *B*-state vibrational energy levels studied here, $10 \leqslant v' \leqslant 20$. We estimate the non-adiabatic coupling assuming a Landau–Zener two-state model for the avoided crossing, where the potential coupling matrix elements in the diabatic basis are equal to half the energy gap between the two adiabatic states at the avoided crossing.

The diabatic couplings as a function of intermolecular geometry are determined by repeating the above procedure for $\gamma = 55°, 60°, 70°$ and 80° and 3.0 Å $\leqslant R \leqslant$ 5.0 Å with a grid size of 0.25 Å. This range of angles and distances covers the most important regions of the intermolecular potentials sampled by the *T*-shaped Ne–Br_2 complex when undergoing direct vibrational predissociation from the *B* state.

The dependence of the couplings on intermolecular angle γ and distance *R* are then fit to analytical expressions. The dependence of the $B/2_g$ couplings are fit to the expression

$$V_{B/2_g}(r, R, \gamma) = \Delta \exp^{-\alpha(R-\rho_e)} \sin\gamma \cos^2\gamma. \quad (1)$$

Consistent with a Landau–Zener type process, there is no dependence on the Br-Br distance *r*. The angular dependence is analogous to that obtained from a diatomics-in-molecules (DIM) model on ArI_2 [10]. A very similar expression is used to fit the *B*/*C* coupling data, but we found that assuming a $\sin\gamma\cos\gamma$ angular dependence led to a better representation of the data. In general the accuracy of the fit is similar to that found on our previous work on $NeCl_2$ [6]: very good for moderate displacements from the equilibrium *T*-shape in both intermolecular degrees of freedom. The fit loses quality for repulsive regions where the two-state model used to extract the couplings is no longer valid. This has little effect on the dynamics which is governed by the Franck–Condon region around the equilibrium geometry. The parameters used to fit the potential energy surfaces and couplings are summarized in Table 1.

The *ab initio* methodology used for calculating the potential energy curves and the spin–orbit eigenvector information discussed above has been described in our previous study on $NeCl_2$ and will only be summarized here. For each Br atom, the 28 core electrons are replaced with the relativistic effective core potential (RECP) of the Stuttgart group which include the spin–orbit coupling terms [25]. The AVTZ basis is used for the valence electrons and is extended with a set of g functions, giving a final basis of *4s4p3d2f1g*. All electrons of the Ne atom are represented explicitly with the AVTZ basis. The molecular orbitals are optimized using a complete active space self-consistent field procedure (CASSCF), with the active space defined by the Br_2 14 valence electrons and the corresponding valence molecular orbitals, together with a state-averaging of thirteen electronic states close in energy to the spectroscopic states under study. Next, a multi-reference configuration interaction (MRCI) calculation is performed, including Davidson's correction for each of the electronic states. Note that at this stage the valence electrons of the Ne atom become correlated. Finally, 36 spin–orbit states of the $NeBr_2$ complex are found by diagonalizing the total (electronic+spin) Hamiltonian using the MRCI wavefunctions as the basis. All calculations are performed using the Molpro 2009.1 package [26].

Table 1
Parameters used in the fit of the potential energy surfaces and couplings developed in the present work. The electronic couplings for the $B/2_g$ coupling is given by Eq. (1). The *B*/*C* couplings are similar with the only change that the angular part takes the form $\sin\gamma\cos\gamma$. The diagonal terms are expressed in the form $V_\beta(r, R, \gamma) = V_\beta(r) + \sum_{i=1,2} D_\beta \left(e^{-2\alpha_\beta(R_i - R_e^\beta)} - 2e^{-\alpha_\beta(R_i - R_e^\beta)} \right)$ with $\beta = B, 2_g$ and *C* states, and R_i being the distance between the Ne atom and the *i*th Br atom.

β	r_e (Å)	Δ (cm^{-1})	α($Å^{-1}$)
B	3.9	42	1.67
C	3.9	46.2	1.67
2_g	3.9	50.4	1.67
B/*C*	3.25	38	3.35
$B/2_g$	3.525	475	2.75

3. Test calculations on the intermolecular potentials for the *B*, *C* and 2_g spin–orbit states

In our previous study on the competition between vibrational and electronic predissociation for $NeBr_2$ we assumed that the intermolecular potentials for the *B*, *C* and 2_g states would be very similar and thus used the empirical potential for the *B* state to represent all of them. We now perform *ab initio* calculations to test this hypothesis and to improve our description of the intermolecular forces in this system. In order to obtain the most reliable *ab initio* description we divide the problem in two independent parts: (a) the accurate calculation of the electronic part of the intermolecular potential (b) an analysis of how to best include the spin–orbit effects, to be discussed next.

We fix the geometry of the complex to the usual *T*-shape characteristic of the ground and *B* states. The main electronic components of the *B*, *C* and 2_g states are: $^3\Pi_u$, $^1\Pi_u$ and $^3\Pi_g$ where the states of the complex are labeled according to their diatomic parentage. Within the C_{2v} symmetry adopted the Π states split into different components: $^3A_1$,$^3B_1$, $^1A_1$, $^1B_1$, $^3B_2$ and $^3A_2$, respectively. The distribution of the different excited states into all of the possible irreducible representations allows one to treat them as ground states in their own spin and spatial symmetry. This is a key technical detail because it allows us to use the most reliable practical method for weak intermolecular forces: coupled-cluster singles and doubles with perturbative correction for triples (CCSD (*T*)). Therefore in the case of the triplet states we apply RCCSD (*T*) as the method of choice. In the case of the singlet states, the $^1A_1$ component corresponds to the first excited state of that spin and spatial symmetry and a different strategy has to be devised. We resort to multiconfigurational methods to calculate the $^1A_1$, $^1B_1$ states specifically the multireference second order perturbation method (MRPT2) and the multireference average coupled pair functional approach (MRACPF). Both of these compare favorably with the multireference configuration interaction approach (MRCI) for describing dispersion bound complexes [27]. Compared with the higher correlated coupled cluster approach the multiconfigurational approaches generally underestimate the binding energies. To obtain a better description of the singlet states we adopt a mixed approach which has proven fruitful in other van der waals systems: the potential obtained at the multiconfigurational level is corrected by adding to it the difference in the potentials obtained at the coupled cluster and multiconfigurational levels for the corresponding (A_1 or B_1) triplet states. The approximation should work quite well given the great similarity in electronic structure between the singlet and triplet A_1 and B_1 components, given that they correspond to the same main electronic configuration and the only difference is the final spin coupling between the two open-shell π_g and σ_u orbitals. From preliminary calculations on the triplet states using the three methods we find, as expected, that RCCSD (*T*) leads to the largest binding energies, MRPT2 leads to binding energies which are roughly 15% smaller and MRACPF to slightly smaller binding energies than MRPT2. For this reason we use the MRPT2 estimates to obtain the correction for the final electronic potentials.

The accurate description of the dihalogen excited states requires the inclusion of spin–orbit effects. This is especially true in order to obtain the proper dissociation limits for the different spin–orbit states and also for the accurate estimates of the state crossings and their non-adiabatic couplings. In principle spin–orbit intermolecular effects can also be expected for the dihalogen weakly bound complexes through configuration interaction mixing. In order to

decide the best way to take into account these effects we performed preliminary MRCI calculations including spin–orbit interactions for the $NeBr_2$ complex. The calculations were performed again for the *T*-shape geometry for two values of the dihalogen distance $r = 2.675$ Å and $r = 3.1$ Å which correspond to the *B* state equilibrium distance and the crossing point between the *B* and 2_g states, respectively, and for several values of the intermolecular distance *R* covering the well region of the weakly bound complex. We use these calculations to analyze the spin–orbit eigenvectors corresponding to the *B*, *C* and 2_g states and quantify the contribution of the different electronic states. Recall that for the isolated dihalogen the spin–orbit states can be labeled by the projection of the total electronic angular momentum, Ω, so that to the *B*, *C* and 2_g states there corresponds Ω values of 0, 1, 2 respectively. This means that both *C* and 2_g states represent one spin–orbit component of a doubly degenerate pair but of course the degeneracy can be lifted upon complex formation. The *B* state main electronic components are the $^3A_1$ and $^3B_1$ states with equal weights, as expected. The first spin–orbit component of the *C* state contains one main electronic contribution: the first excited $^1A_1$ electronic state. The second spin–orbit component contains also one main contribution corresponding to the $^1B_1$ electronic state. Finally, the 2_g state contains two main electronic components, $^3B_2$ and $^3A_2$, with equal weights. In all cases the mentioned main components represent roughly 90% of the total wavefunction.

The above analysis suggests a simple procedure for including spin–orbit effects in the calculation of the intermolecular potentials for the states involved: the *B* state potential can be obtained as an average of the $^3A_1$ and $^3B_1$ purely electronic potentials, the *C* states potentials can be represented by the purely electronic $^1A_1$ and $^1B_1$ states and finally the 2_g state potential can be obtained as an average of the $^3B_2$ and $^3A_2$ purely electronic potentials. The great advantage of this choice is that we can use the most reliable RCCSD (T) electronic potentials to build up the proper spin–orbit intermolecular potentials. It should be noted that of the two degenerate spin–orbit components to which both the *C* and 2_g states belong only one for each of them can couple through non-adiabatic matrix elements with the *B* state for symmetry reasons: when the degeneracy of these pairs is lifted by interaction with the noble gas the general symmetry is lowered to C_s and these pairs now split into *A*' and *A*'' symmetries, since all the vibrational modes and the *B* state are of *A*' symmetry only the *A*' components can be coupled. The *A*'' components could couple through rotational degrees of freedom but we neglect them in this work and previous studies have shown that indeed these couplings are small [7].

4. Dissociation dynamics method

The $NeBr_2$ complex fragments as $Ne+Br_2$ in the *B* state, and as Ne+Br+Br in all the other Br_2 dissociative electronic states. For treating these dissociation pathways, we use Jacobi vectors **r**, the intramolecular Br-Br vector, and **R**, the vector joining Ne to the center of mass of Br_2. The fragmentation dynamics is considered to be nearly independent on total angular momentum, *J*, and for this reason $J = 0$ will be considered. In principle there are combined rotational/electronic terms which could couple Br_2 rotational states with different total helicity projection and electronic states with different electronic helicities, such as the *B* and *C* states. Although for $J > 0$ such couplings are nonzero they are not expected to change dramatically the electronic predissociation which is mainly driven by the non-adiabatic couplings induced by the rare gas atom. The coriolis couplings are of second order and could be important when the spin–orbit states are nearly degenerate, i.e., at the diatomic dissociation limit. However in our case the coriolis coupled states are a bound *B* state and a dissociative *C* state with different dissociation limits and therefore are expected to only add minor corrections to the dominant non-adiabatic couplings calculated in this work. The wave-packet method used has been described previously [5,14] and only some technical details are provided here. For $J = 0$, the total wave packet is expanded as

$$\Psi_t = \sum_e |e\rangle \quad \Phi_e(R, r, \gamma; t), \tag{2}$$

where $|e\rangle$ are the electronic states described above. The three internal coordinates *r*, *R* and γ are described in grids. A two-dimensional grid of 256×160 points are used for the radial variables in the intervals $1.5 < r < 7$ Å, and $2.5 < R < 18$ Å. The angle γ is described by 35 Gauss–Legendre quadrature points in the interval $[0, \pi/2]$.

A Chebyshev propagator is used, with a time interval of 20 fs up to, typically, several hundreds of picoseconds when the dissociation of the complexes is complete. After each time step, the wave packet is multiplied by an absorbing gaussian for $r > 5$ Å, and $R > 15$ Å, with exponential constants of 0.05 and 0.025 for *r* and *R*, respectively.

The initial state corresponds to the ground van der Waals state for each $Br_2(B, v')$ vibrational level. It is calculated using only the $Br_2(B)$ state. First, the vibrational state $\varphi_v(r)$ of the $Br_2(B)$ fragment is calculated numerically at very long $Ne–Br_2$ distances. This function is used to calculate the $\int dr \varphi_v(r) V^B(r, R, \gamma) \varphi_v(r)$ matrix element. Finally, the resulting two-dimensional Schrödinger equation is represented in a basis set and diagonalized for each v'. The ground state obtained is then represented in the grid used for the wave packet propagation.

The wave packet propagation considers the 3 electronic states described above. At each time, the autocorrelation function $\langle \Psi_{t=0} | \Psi_t \rangle$ is calculated providing information on the decay of the initial state. The auto-correlation function is fitted to an exponential $e^{-\Gamma t/\hbar}$, where Γ is the total decay constant, associated to the lifetime $\tau = \hbar/2\Gamma$ of each state. The population on each electronic state, $P_e(t)$, is calculated at each time, incorporating the flux absorbed. This quantity provides a quantification of the EP on the different electronic states. This function is fitted to $Q_e e^{-\Gamma t/\hbar}$, where $Q_e = \Gamma_e/\Gamma$ is the branching ratio of each state. As will be described in the next section the functions assumed both for the autocorrelation function and the electronic state populations provide reliable fits.

5. Results and discussion

Our calculation of the intermolecular potentials for Ne interacting in the perpendicular configuration with the *B*, *C* and 2_g states of Br_2 are shown in Fig. 1. In Fig. 1a, the Br-Br distance, $r = 2.675$ Å, is the equilibrium value while in Fig. 1b results are shown for a stretched Br-Br bond, $r = 3.1$ Å. In our previous work, these three potentials were assumed to be the same. Here, we see that while they are similar, there are important differences between them. For the equilibrium Br_2 distance, the most notable differences are that the well for the 2_g state is 25% deeper and at a 0.25 Å shorter *R* value than for the other two states. As the Br_2 bond stretches, both the *B* and *C* state distances move toward that of the 2_g state. The well depth for the *C* state increases the most, and approaches that of the 2_g state.

For the dynamical calculations, we use a hybrid of the *ab initio* and empirical potentials. We use the empirical *B* state potential, and adjust the other two so that the differences between the three are in closer accord with the *ab initio* results. Specifically, we adjust the 2_g state to be 20% more attractive and the *C* state to be 12% more attractive than the *B* state. In Table 2 we summarize the equilibrium properties of the van der Waals interaction potentials as obtained from the present *ab initio* test calculations, those used in our previous study [24] and those of the present work.

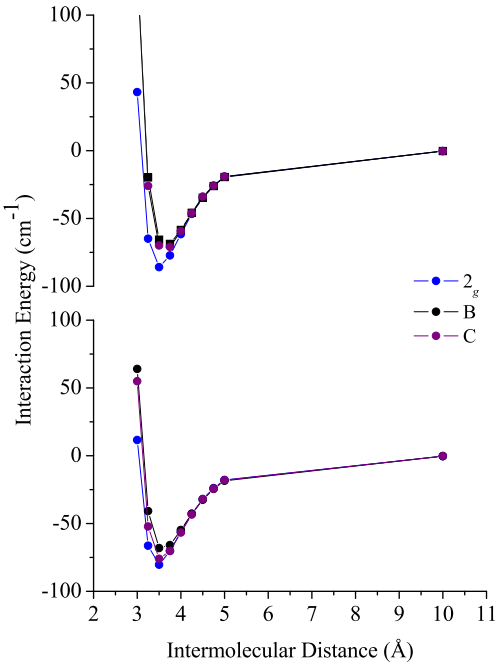

Fig. 1. Intermolecular potentials for the *B*, *C* and 2_g states for (a, top) $r = 2.675$ and (b, bottom) $r = 3.1$ Å.

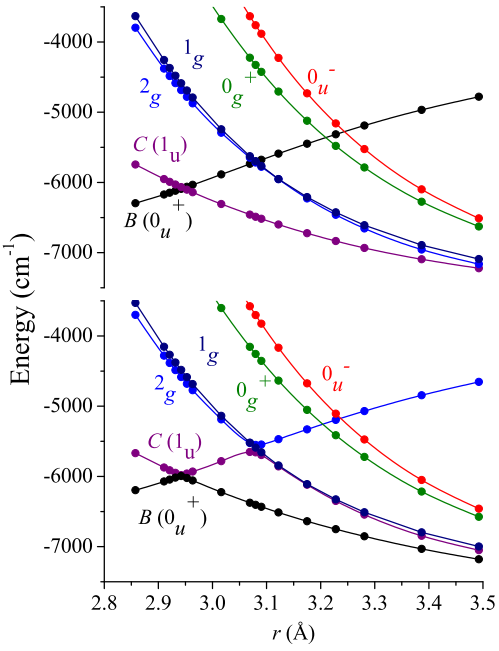

Fig. 2. $NeBr_2$ potential energy curves as a function of Br-Br internuclear distance calculated with the Ne atom fixed at (a, top) $R = 4.50$ Å, $\gamma = 60°$ and (b, bottom) $R = 3.75$ Å, $\gamma = 60°$.

Next, we present the non-adiabatic coupling results. The Br-Br potential energy curves calculated with the Ne atom fixed at $R = 4.50$ Å, $\gamma = 60°$ are shown in Fig. 2a. The curves are labeled using the term symbols of the free Br_2 states to which the curves correlate at large *R*. As is evident in the Fig. 2a, the Ne–Br_2 interaction does not lead to any significant coupling between the *B* state and the repulsive states for this geometry; the curves cross as in free Br_2. For $R = 3.75$ Å, $\gamma = 60°$, shown in Fig. 2b, on the other hand, the van der Waals interaction leads to a significant avoided crossing between the *B* and 2_g states. For this particular geometry, the fit to the curves yields a coupling strength $V_{B/2_g} = 53$ cm^{-1}. Similar calculations and fits were performed for a variety of geometries, and the results are illustrated in Fig. 3.

As seen in Fig. 3, the *B*/*C* coupling is not negligible, but is much weaker than the $B/2_g$ coupling. This can be easily explained on the basis of the electronic parentage of the spin–orbit states involved. In the case of the *B* and 2_g states the coupling is mainly due to the interaction between the $^3\Pi_u$ and $^3\Pi_g$ primary electronic components, whereas for the *C* state the main electronic component, $^1\Pi_u$, cannot directly interact and relies on its secondary triplet components which mix in as a consequence of spin–orbit coupling. In short, the *B*/*C* coupling is a consequence of spin–orbit effects while the $B/2_g$ coupling is due to the *g*/*u* spatial symmetry breaking induced by the neon atom.

Given the inherent difficulty in calculating non-adiabatic couplings for weakly interacting systems, and the inherently underdetermined fit used in the previous study, the agreement between the *ab initio* results presented here and the empirical fit is remarkable. The calculated $B/2_g$ coupling is 5% smaller than that previously assumed. The *B*/*C* coupling is more difficult to compare due to the different functional forms that were used for the two studies. For $\gamma = 80°$ the calculated coupling is 5% stronger than that previously assumed for *R* values close to the Franck Condon region.

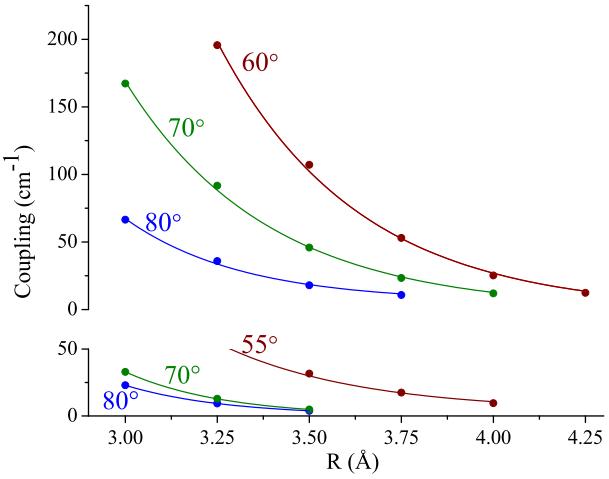

Fig. 3. Top: Estimated diabatic $B/2_g$ coupling as a function of intermolecular distance *R* and angle γ. Bottom: Estimated diabatic *B*/*C* coupling as a function of intermolecular distance *R* and angle γ.

Table 2
Equilibrium properties for the *B*, *C*, and 2 g intermolecular potentials. The first two columns correspond to the *ab initio* test calculations for the equilibrium Br–Br distance in the *B* state and for a stretched value corresponding to the crossing point between the *B* and 2 g states. The third column corresponds to the potentials used in our previous model study Ref. [22] and the last column are those of the present work.

	Ab initio $r = 2.675$ Å		Ab initio $r = 3.1$ Å		Previous model study, Ref. [22]		Present work	
	R_e	D_e	R_e	D_e	R_e	D_e	R_e	D_e
B	3.65	70	3.55	69	3.67	84	3.67	84
C	3.65	73	3.50	76	3.67	84	3.67	93
2 g	3.45	86	3.45	81	3.67	84	3.67	100

As R decreases, the calculated coupling becomes smaller than that previously assumed.

It is also interesting to compare our *ab initio* results to those of the DIM models that have been very useful for previous studies. Buchachenko and coworkers have reported [28,29] intermolecular potentials and diabatic couplings for the B and 2_g states of $NeBr_2$ based on accurate *ab initio* calculations for the diatomic fragments [30]. They predict similar intermolecular equilibrium distances and 10% stronger binding energies compared to those presented here. However, the $B/2_g$ couplings predicted by the DIM model are much smaller (by a factor of 3–5) than the *ab initio* results, especially for longer intermolecular distances. The couplings calculated with the DIM model vary somewhat more as a function of γ. It is clear that the DIM couplings would not be strong enough to account for the observed EP rates. We speculate that the couplings calculated by DIM are too weak due to the insufficient inclusion of spin–orbit effects. A more advanced DIM model was applied to the Rg-I_2 complexes [10] and it would be interesting to test that model for $NeBr_2$.

The intermolecular potentials and couplings described above were used to perform wave packet dynamical calculations for $NeBr_2$ B state vibrational levels $8 \leqslant v' \leqslant 23$. The probability that the Br_2 remains in its initially populated v' level as a function of time for each level is illustrated in Fig. 4 for selected vibrational levels, along with a single exponential fit to the results for each level. Up to $v' = 22$ the single exponential fits are quite robust, indicating simple first-order coupling between the initial state and the manifold of final states. Starting at $v' = 23$, IVR dynamics sets in due to the closing of the $\Delta v = -1$ vibrational predissociation channel.

Fig. 5 shows the lifetimes versus Br_2 B state vibrational level obtained from exponential decays such as displayed in Fig. 4. The previous experimental data [31] and empirical fit results [24] are also shown for comparison. Although the specific vibrational dependence varies between the three studies, the newly calculated lifetimes are in comparable agreement with the data as were the previous empirically fitted lifetimes. With the exception of $v' = 11$, the EP modulation of lifetime versus vibrational level is somewhat larger for the *ab initio* calculation than for the data. Both the new potential and the previous one predict that the EP process results in quite short lifetimes for $v' = 8$ and 9. The calculations presented here extend the results up to $v' = 23$, and an interesting increase in the lifetime is observed for that level. The fit in Fig. 4 shows that this state does not undergo exponential decay, and thus the lifetime is not rigorous. This issue has been discussed thoroughly in Ref. [32].

The EP branching ratios to the two possible electronic manifolds as a function of initial vibrational level are shown in Fig. 6. The contribution of the 2_g state oscillates as a function of v'. The EP

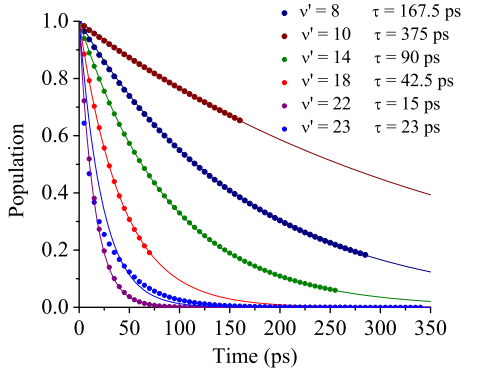

Fig. 4. Square of the autocorrelation function or initial state population as a function of time for some selected v' (points) and analytical fits (solid lines) to $e^{-t/\tau}$. (For interpretation of the references to colour in this figure legend, the reader is referred to the web version of this article.)

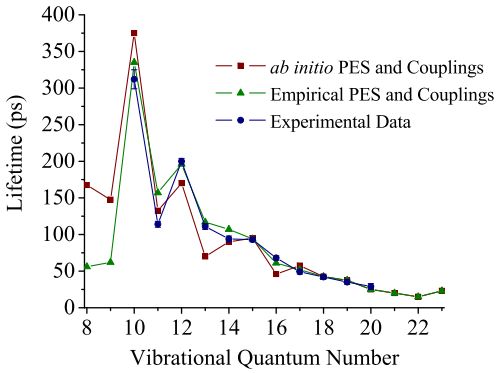

Fig. 5. Lifetimes as a function of initial vibrational excitation of Br_2 obtained for (a) the *ab initio* based PES's of this work, (b) the semi-empirical PES's of Ref. [24], (c) the experimental values of Ref. [31].

contribution increases as the VP rate decreases, but for certain levels the EP rate is very small. In our previous study, we showed that this closely correlates with the Franck–Condon factor between the initial B state Br_2 stretching wave function with the product translational functions on the 2_g potential. The increase in branching to the 2_g state for $v' = 23$ could result from an anomalously slow VP rate for that level, but could also be due to the greater sampling of strong-coupling geometries due to IVR. The EP rate to the C state has a smoother dependence on vibrational level, again as predicted by Franck–Condon overlap. The C state branching ratio decreases for level for which coupling to the 2_g state is especially strong, especially for $v' = 8$ and 9. Other than the Franck–Condon factors, the ratio of coupling to 2_g and C is roughly consistent with the ratio of the coupling strengths presented in Fig. 3.

As previously discussed, this is the first case for which EP in a Rg-X_2 van der Waals dimer has been observed to be in competition with direct vibrational predissociation. It is very satisfying that the agreement between experiment and theory is excellent for this problem. We are especially satisfied that the *ab initio* results presented here are in accord with both the empirical fit and with the data. This good agreement suggests that the poor agreement obtained in previous studies of $NeCl_2$, $ArCl_2$ and ArI_2 is mainly due to the hypersensitivity of the IVR rate to the minute details of the assumed potential. IVR depends on "coincidental" resonances between the initially populated van der Waals mode and high van der Waals levels of the halogen $v' - 1$ stretching mode, so the potential surface would need to be very precisely determined to obtain the correct IVR rate. Now that we know that the electronic coupling can be reasonably well calculated, this gives us hope that the complete problem might be "solvable" for the competition between electronic coupling and IVR.

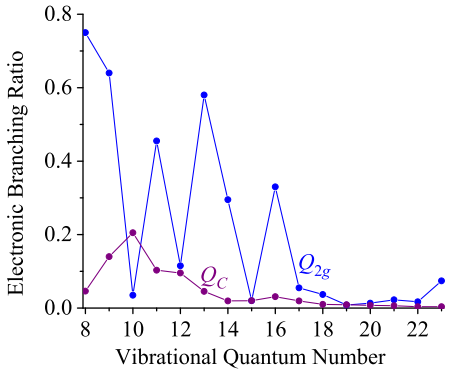

Fig. 6. Branching ratio for the 2_g and C electronic states as a function of initial vibrational excitation of Br_2 obtained with the *ab initio* based PES's of this work.

For $NeBr_2$, several follow on experiments would be very useful. First, experimental studies of both the lower and higher vibrational levels would add significant insight. Studies of $v' = 7$, 8 and 9 would help confirm the conclusions we have reached in the present study. Unfortunately, such experiments are quite difficult due to small Franck Condon factors for the excitation transition, especially since we are using Br_2 product detection as our main signal. Detection of Br atom products would help alleviate this problem. Detection of atomic products for the higher vibrational levels would also be extremely useful since the lifetimes for these levels are in the range of the pulse length of our current laser system. A somewhat faster laser would also be useful in this regard. Accurate branching ratio measurements for the high vibrational levels of $NeBr_2$ would also be very useful for observing the effect of IVR on the electronic dynamics. Previously we have speculated that the EP rate should dramatically increase with IVR since geometries for which the coupling is strong are more heavily weighted once resonances with high van der Waals vibrational modes are important.

The excellent agreement obtained here also suggests that a theoretical study of $ArBr_2$ would be quite interesting. The experimental data for this molecule suggests that the EP rates are higher than the VP rates for most levels, but this makes it difficult to estimate the branching ratios for any level because there is no level for which VP clearly predominates and can be used to scale the results. On the other hand the *ab initio* calculations for $ArBr_2$ would be of similar difficulty to those presented here if only the valence electrons are included in the correlated calculations, thus making its computational treatment amenable.

The work presented here should also provide a motivation to reexamine both Rg-I_2 and Rg-Cl_2 dimers. As shown in Fig. 7 the regions of the curve crossing for Cl_2, Br_2 and I_2 are quite different due to the different values of the spin–orbit coupling. For Cl_2, the crossings start 2/3 of the way up the well, at nearly 1 Å $Cl - Cl$ stretching amplitudes. This gives rise to the phenomenon, for instance, that for $ArCl_2$ $v' = 12$ VP still dominates the dynamics whereas for higher vibrational levels VP can not be observed because EP dominates. For $NeCl_2$ and $HeCl_2$, the onset of EP dynamics with increasing vibrational level appears to be quite sharp from the available data, but this is not consistent with the theory, especially for $NeCl_2$. Better data, especially product atom detection, would be extremely useful for the Rg-Cl_2 dimers. Similarly, extending the data to lower vibrational levels for the Rg-Br_2 dimers would also be very interesting since the curve crossings in this case are much lower in the potential, and vary much more with the identity of the crossing curve. For instance, the curve crossing for the *C* state is 250 cm^{-1} lower in energy and for 0.3 Å shorter bond lengths than that of the 2_g state. Therefore we would expect the *C* state to dominate the EP branching ratios for the lower vibrational levels.

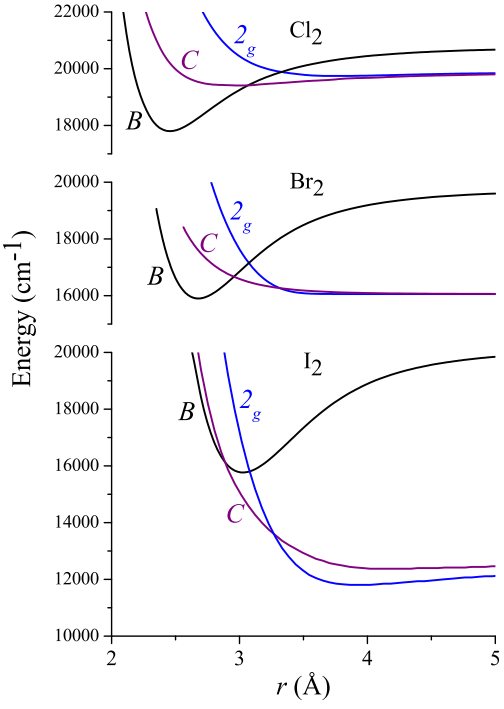

Fig. 7. Potential energy curves of the *B*, *C* and 2_g electronic states of Cl_2, Br_2 and I_2.

Of course, the most heavily studied example of the competition between VP and EP is for the ArI_2 molecule, yet there is still poor agreement between experiment and theory. The results of this study suggest that the calculation of the EP rate in this case may be reasonably accurate, and that the poor comparison between experiment and theory is mostly due to the lack of quantitative results for IVR-VP, for reasons discussed above. As shown in Fig. 7, the curve crossings for the case of I_2 are near the equilibrium internuclear distance, and thus the energy level of the crossing is quite insensitive to the identity of the product state, and the *r* value varies significantly. Again detection of the atomic products for these dimer would add significant new insight. Detection of atomic products for NeI_2 and HeI_2 would also be very interesting. It may be that the possible role of EP for these dimers have been neglected for the simple reason the VP signals are so strong that it EP did not need to be invoked to explain weak signals. The ArI_2 results suggest that the EP rate does not vary so much with vibrational level that an oscillation, such as observed here, would reveal the importance of an EP channel.

Finally, we note that higher n Rg_n-X_2 cluster experiments have been analyzed while mostly ignoring the possibility of the EP channel. [33] The detailed understanding of the case of $NeBr_2$, presented here, suggests that Ne_2Br_2 would be an especially interesting example for further study. In this case, the competition between the various VP channels has been more completely characterized than for any analogous cluster. However, the role of EP has yet to be explored. Such experiments will be quite complex, but the results would be fascinating.

6. Conclusions

We have presented an *ab initio* study of the Ne–Br_2 potential energy surfaces and the non-adiabatic couplings between the valence excited electronic states. The calculations show that the intermolecular potentials of the *B*, *C* and 2 g states have similar intermolecular equilibrium distances and binding energies, as assumed in our previous model study [24], but quantitative differences exist, most notably a larger binding energy for the 2 g state. These *ab initio* results were used to obtain 3-D approximate potentials for each electronic state, and these potentials were used in a wave packet calculation of the competing EP and VP dynamics. The results of this calculation are in excellent agreement with both experimental results [31] and a previous empirical fit [24] to the experiments. The ability of *ab initio* coupling surfaces to so accurately reproduce experimental data raises the hope of a complete understanding of the VP and EP dynamics for each of the $Rg - X_2$ dimers.

The present study suggests that a key element to understand the competition between EP, VP and IVR in the $Rg - X_2$ systems is the relative location of the crossing points between the three states involved and their drastic variation in the halogen series. In this sense prevailing discrepancies between theory and experiment for other related $Rg - X_2$ systems are most likely due to the subtle dependence of IVR dynamics on the properties of the potential energy surface. On the other hand, the present work suggests the need to perform additional experimental measurements, in

particular, we predict that for $v = 8,9$ EP will again dominate the decay dynamics. In the case of the higher n Rg_n-X_2 clusters the importance of the EP processes is unknown. Thus, much work still remains to be done on these fascinating systems.

Acknowledgments

The authors thank Professor A.A. Buchachenko for many useful comments and kindly providing a subroutine to evaluate the DIM potentials and couplings. This work has been supported by the Ministerio de Ciencia e Innovación under grants CSD2009–00038 (programa CONSOLIDER-INGENIO 2010 entitled "Molecular Astrophysics: the Herschel and Alma era"), and FIS2010-18132, US National Science Foundation Grant CHE-0911686. The *ab initio* calculations were performed at UCI's department of chemistry computational facilities. The dynamical calculations have been performed in the IFF and CESGA computing centers.

References

[1] A. Rohrbacher, N. Halberstadt, K.C. Janda, Annu. Rev. Phys. Chem. 51 (2000) 405.
[2] G. Kubiak, P.S.H. Fitch, L. Wharton, D.H. Levy, J. Chem. Phys. 68 (1978) 4477.
[3] D.H. Levy, Adv. Chem. Phys. 47 (1981) 323.
[4] O. Roncero, N. Halberstadt, J.A. Beswick, J. Chem. Phys. 104 (1996) 7554.
[5] O. Roncero, A.A. Buchachenko, B. Lepetit, J. Chem. Phys. 122 (2005) 034303.
[6] C.R. Bieler, K.C. Janda, R. Hernández-Lamoneda, O. Roncero, J. Phys. Chem. A 114 (2010) 3050.
[7] Y. Asano, S. Yabushita, J. Phys. Chem. A 105 (2001) 9873.
[8] A. Rohrbacher, J. Williams, K.C. Janda, Phys. Chem. Chem. Phys. 1 (1999) 5263.
[9] D.S. Boucher DS, R.A. Loomis, Adv. Chem. Phys. 138 (2008) 375.
[10] A.A. Buchachenko, N. Halberstadt, B. Lepetit, O. Roncero, Int. Rev. Phys. Chem. 22 (2003) 153.
[11] M.L. Burke, W. Klemperer, J. Chem. Phys. 98 (1993) 6642.
[12] J.J. Breen, D.M. Willberg, M. Gutmann, A.H. Zewail, J. Chem. Phys. 93 (1990) 9180.
[13] O. Roncero, S.K. Gray, J. Chem. Phys. 104 (1996) 4999.
[14] B. Lepetit, O. Roncero, A.A. Buchachenko, N. Halberstadt, J. Chem. Phys. 116 (2002) 8367.
[15] N. Goldstein, T.L. Brack, G.H. Atkinson, J. Chem. Phys. 85 (1986) 2684.
[16] C.R. Bieler, K.C. Janda, J. Am. Chem. Soc. 112 (1990) 2033.
[17] C.R. Bieler, K.E. Spence, K.C. Janda, J. Phys. Chem. 95 (1991) 5058.
[18] J.I. Cline, N. Sivakumar, D.D. Evard, K.C. Janda, Phys. Rev. A 36 (1987) 1944.
[19] J.I. Cline, B.P. Reid, D.D. Evard, N. Sivakumar, N. Halberstadt, K.C. Janda, J. Chem. Phys. 89 (1988) 3535.
[20] J.I. Cline, N. Sivakumar, D.D. Evard, K.C. Janda, J. Chem. Phys. 86 (1987) 1636.
[21] J.I. Cline, N. Sivakumar, D.D. Evard, C.R. Bieler, B.P. Reid, N. Halberstadt, S.R. Hair, K.C. Janda, J. Chem. Phys. 90 (1989) 2606.
[22] D.D. Evard, C.R. Bieler, J.I. Cline, N. Sivakumar, K.C. Janda, J. Chem. Phys. 89 (1988) 2829.
[23] R. Hernández-Lamoneda, K.C. Janda, J. Chem. Phys. 123 (2005) 161102.
[24] C. Sanz-Sanz, O. Roncero, R. Hernández-Lamoneda, J.M. Pio, M.A. Taylor, Kenneth C. Janda, J. Chem. Phys. 132 (2010) 221103.
[25] A. Bergner, M. Dolg, W. Kuechle, H. Stoll, H. Preuss, Mol. Phys. 80 (1993) 1431.
[26] H.-J. Werner , P.J. Knowles, R. Lindh, F.R. Manby, M. Schutz, et al., Molpro, version 2009.1, a package of ab initio programs (2009).
[27] M. Bartolomei, M.I. Hernández, J. Cámpos-Martínez, E. Carmona-Novillo, R. Hernández-Lamoneda, PCCP 10 (2008) 5374.
[28] A.A. Buchachenko, N.F. Stepanov, J. Chem. Phys. 104 (1996) 9913.
[29] A.A. Buchachenko, O. Roncero, N.F. Stepanov, Russ. J. Phys. Chem. 74 (2000) S193.
[30] A.A. Buchachenko, T.A. Grinev, T.G. Wright, L.A. Viehland, J. Chem. Phys. 128 (2008) 064317.
[31] M.A. Taylor, J.M. Pio, W.E. van der Veer, K.C. Janda, J. Chem. Phys. 132 (2010) 104309.
[32] A. García-Vela, K.C. Janda, J. Chem. Phys. 124 (2006) 034305.
[33] J.M. Pio, M.A. Taylor, W.E. van der Veer, C.R. Bieler, J.A. Cabrera, K.C. Janda, J. Chem. Phys. 133 (2010) 014305.